



**HAL**  
open science

# Numerical investigation of the unsteadiness of a fan tip-leakage vortex

Jérôme Boudet

► **To cite this version:**

Jérôme Boudet. Numerical investigation of the unsteadiness of a fan tip-leakage vortex. 2017. hal-01576613

**HAL Id: hal-01576613**

**<https://hal.science/hal-01576613>**

Preprint submitted on 23 Aug 2017

**HAL** is a multi-disciplinary open access archive for the deposit and dissemination of scientific research documents, whether they are published or not. The documents may come from teaching and research institutions in France or abroad, or from public or private research centers.

L'archive ouverte pluridisciplinaire **HAL**, est destinée au dépôt et à la diffusion de documents scientifiques de niveau recherche, publiés ou non, émanant des établissements d'enseignement et de recherche français ou étrangers, des laboratoires publics ou privés.

# Numerical investigation of the unsteadiness of a fan tip-leakage vortex

Jérôme Boudet\*

*Univ Lyon, Ecole Centrale de Lyon, CNRS, LMFA, F-69134, Ecully, France*

## Abstract

The movement of the tip-leakage vortex in a fan flow is investigated, from data of an existing zonal large-eddy simulation. A methodology is presented to analyze the motion of the vortex, using low-pass filtering and integral-based vortex identification functions. This approach permits to focus on the largest vortices of the flow at each instant, through normalized criteria. In the present fan flow, the velocity spectra are characterized by a peak frequency associated with a natural unsteadiness, in the casing region downstream of the rotor blades. Using the present methodology, in a plane just downstream of the blade trailing edge, a significant wandering motion of the vortex is shown. Further downstream, where the vortex interacts with the adjacent blade wake, the vortex movement is much more disordered. This is interpreted as a vortex splitting phenomenon. But when only the mean flow and the peak frequency are retained in the analysis, a wandering motion is observed again.

**fan / tip-leakage / vortex wandering / vortex identification functions**

---

\*jerome.boudet@ec-lyon.fr

## Nomenclature

DFT	discrete Fourier transform
DLR	Deutsches Zentrum für Luft- und Raumfahrt
$f$	frequency
$h$	clearance height
LES	large-eddy simulation
$P_0$	total pressure
PIV	Particle Image Velocimetry
RANS	Reynolds-averaged Navier-Stokes
$R_c$	casing radius
$U_{tip}$	blade tip velocity
$y_2, z_2$	local coordinates attached to each analysis window
$\Gamma_1, \Gamma_2$	vortex identification functions
$\eta$	isentropic efficiency of the rotor

## 1 Introduction

Flows in turbomachines (fans, compressors, turbines...) are characterized by different vortices developing through the blade and vane passages (see Lakshminarayana [6]). Among these is the tip-leakage vortex (TLV), which originates from the clearance at the blade or vane tip. It is generally a powerful feature of the flow, associated with vorticity and losses. Concerning the flow stability, Vo *et al.*[11] have shown the TLV trajectory controls the initiation of rotating stall in some compressors. Furthermore, the development of the TLV along the blade tip and past the trailing edge must also affect the noise emission.

The unsteadiness of the TLV is a topic of interest as regards flow stability and noise. In the context of external aerodynamics, Bailey and Tavoularis[1] investigated experimentally the oscillation of a wing-tip vortex in a turbulent flow. This kind of disordered oscillation is generally referred to as "wandering" or "meandering". The recent development of large-eddy simulation (LES) for high-Reynolds number flows, in relation with the increase of computational resources, permitted to identify such a wandering motion in the context of turbomachines, for the TLV. You *et al.*[13] observed this unsteadiness in a cascade configuration, and Pogorelov *et al.*[9] obtained also indications of such a wandering in a rotor. Recently, Particle Image Velocimetry (PIV) permitted to visualize such oscillations in experimental rigs (Tan *et al.*[10], Liu *et al.*[8]). In these experimental references, the TLV is shown to reach even more severe unsteadinesses: "vortex splitting", and even "vortex breakdown" with backflow.

A natural unsteadiness has been observed in the tip flow of a fan by the present author and co-workers, and presented in a recent paper [2]. The main objective of this original publication was to validate a zonal LES simulation of the fan flow, in comparison with detailed experimental data. In particular, a remarkable description of the flow spectrum downstream of the rotor tip was shown, and a natural unsteadiness was pointed out. However, the characterization of the unsteadiness, interpreted as vortex wandering, remained cursory, through a simple analysis of the Fourier transformed radial velocity at a given frequency. The objective of the present paper is to characterize

more precisely the unsteadiness, by an analysis in the time domain, over a range of frequencies, and at two different axial positions.

In section two, the fan flow and the numerical simulation are introduced. The main characteristics are given in this section but the reader is invited to consult the original paper [2] for further information and a detailed validation of the simulation. In the third section, the methodology to analyze the vortex motion is developed. Finally, the methodology is applied in the fourth section, for a detailed characterization of the present tip-leakage vortex.

## 2 Fan configuration and numerical approach

### 2.1 Fan configuration

The configuration has been investigated experimentally by DLR Berlin, in the frame of the EU project FLOCON. It is constituted of a 24-blade rotor and a 32-vane stator. The rotor alone is considered in the numerical study. The casing radius is  $R_c = 228.6$  mm, the rotor chord length is  $c = 43.5$  mm, the maximum blade thickness at tip is 3 mm, the rotor tip clearance is  $h = 2.4$  mm and the rotation speed is 3195rpm. Using the blade tip velocity and the chord length, the Mach number is 0.22 and the Reynolds number is  $2.2 \times 10^5$ .

### 2.2 Zonal large-eddy simulation

Nowadays, in industry, aerodynamic design heavily relies on averaged simulations (RANS). However, for a detailed analysis of the natural unsteadiness of a vortex, the largest turbulent eddies must be described, which calls for an approach such as large-eddy simulation (LES). This approach is computationally expensive at high Reynolds numbers, because the number of grid points has to grow to render a significant part of the turbulent spectrum. Consequently, in the present study, a zonal approach has been employed: LES is used only in the region of interest (near the casing), while RANS is used elsewhere. The eddy viscosity is calculated as:

$$\mu_{mod} = (1 - \beta(\mathbf{x}))\mu_{sgs} + \beta(\mathbf{x})\mu_t$$

where  $\mu_{sgs}$  is the LES subgrid-scale viscosity given by the shear-improved Smagorinsky model [7], and  $\mu_t$  is the RANS turbulent viscosity given by the  $k - \omega$  model of Wilcox [12]. The coupling function  $\beta$  is set to a 4th order polynomial that evolves smoothly from  $\beta = 1$  below  $r = 0.89 \cdot R_c$  to  $\beta = 0$  above  $r = 0.94 \cdot R_c$ .

The numerical resolution has been carried out with the in-house solver *Turb'Flow* [4], a finite-volume vertex-centered solver for multi-block structured grids. The inviscid fluxes are interpolated with a four-point centered scheme, with 4<sup>th</sup> order artificial viscosity (coefficient:  $\leq 0.01$  in the tip region [3]). The viscous fluxes are interpolated with a two-point centered scheme. A three-step Runge-Kutta scheme is used for the time marching, with a time step of  $2.5 \times 10^{-8}$  s =  $4.3 \times 10^{-5} \cdot c/U_{tip}$ . Concerning the grid, in the LES region at tip, the cell dimensions in wall units yield:  $\Delta x^+ < 30$

(streamwise),  $\Delta y^+ < 3$  (wall-normal) and  $\Delta z^+ < 50$  (cross-stream). One blade passage is described, with periodicity. Thanks to the use of the zonal approach, the total number of grid points is moderate:  $11 \times 10^6$ . The analysis below is based on 640 regular instants of the unsteady flow after convergence, over a total duration of nearly  $28 \cdot c/U_{tip}$ .

The computed performances of the fan rotor are presented in Table 1. As shown in reference [2], the operating point has been chosen at an intermediate position, with a mass flow higher than the maximum loading condition, in the more stable part of the operating range.

Table 1: Computed performances of the fan rotor.

Inlet mass-flow $\dot{m}_1$ [kg/s]	3.33
Total pressure ratio $P_{02}/P_{01}$ [.]	1.012
Isentropic efficiency $\eta$ [%]	95.4

A detailed presentation of the computation, and selected comparisons with experimental data, can be found in the original paper [2]. In particular, a remarkable match with the experimental flow spectrum (broadband component and peaks) is observed downstream of the rotor, at  $r = 0.98R_c$ . This is not shown again in the present paper, where the computation is considered as a given database, on which a specific methodology is used to analyze the motion of the TLV. A particular attention is paid to the natural unsteadiness associated with the peak frequency in the rotating frame of reference.

### 3 Methodology to characterize the vortex motion

This section is dedicated to the temporal analysis of the vortex motion. It makes use of 2D cutting windows through the TLV, on which vortex identification functions are calculated.

#### 3.1 Analysis windows

Two analysis windows (labeled AW1 and AW2) are positioned perpendicularly to the TLV, as shown in Figure 1. In this figure, the computed blade passage is repeated twice to locate the windows with respect to the periodic flow field. AW1 corresponds to the early development of the TLV, just downstream of blade (a). AW2 is farther downstream along the TLV, at about  $2.4c$  from the trailing edge of blade (c). It should be recalled here that since only one blade passage is simulated, with azimuthal periodicity, both AW1 and AW2 are actually through the same vortex, at different streamwise positions.

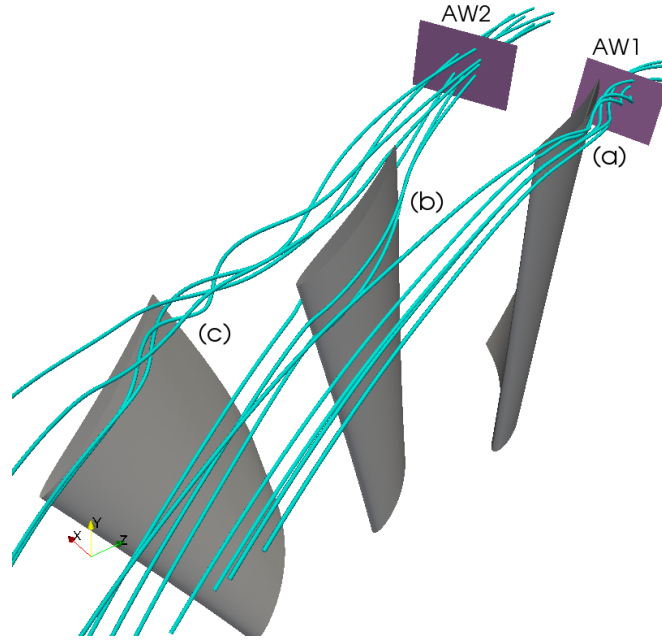
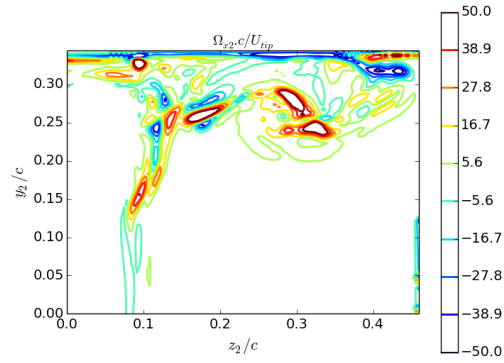


Figure 1: Mean relative streamlines in three adjacent blade passages, and positions of the analysis windows AW1 and AW2.

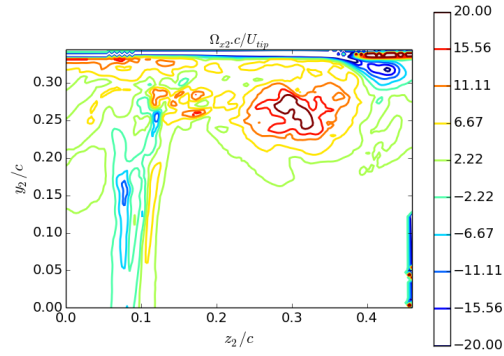
### 3.2 Vortex identification functions

The methodology to characterize the TLV at a given instant is illustrated on the first analysis window (AW1). In the following, the flow is always considered in the rotating frame of reference. An example of instantaneous contours of vorticity is plotted in Figure 2-a), for a given instant. It is difficult to identify the TLV because various turbulent eddies are entrained by the TLV and yield local extrema of vorticity. In order to efficiently track the evolution of the TLV, the unsteady flow has to be low-pass filtered. The Discrete Fourier Transform (DFT) in time of the 2D field is calculated and only the frequencies below  $f_c = 2,200\text{ Hz} = 1.28 \cdot U_{tip}/c$  are retained before the DFT is reversed to obtain the low-pass filtered signal. This cut-off frequency is chosen above the natural frequency (around 1,800 Hz) identified in the previous paper [2] and shown again in the spectra to be presented below (Fig. 4). The contours of vorticity of the filtered flow, at the same instant, are presented in Figure 2-b). The turbulent eddies are smoothed by the filter, and the shape of TLV is now more clearly identified. However, vorticity is a local quantity and is not adapted to gauge a vortex, which is characterized by a spatial coherence. For example, high levels of vorticity are found in the casing boundary layer in Figure 2-b) but do not correspond to a vortex. Consequently, space integral quantities are needed to identify the TLV.

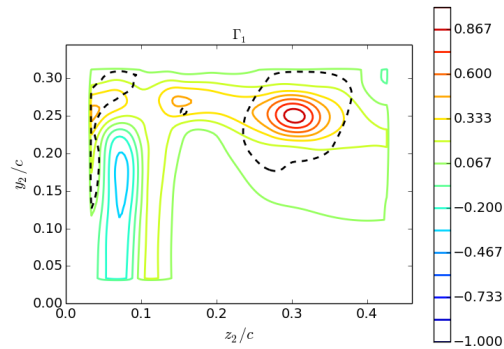
We propose to use the vortex identification functions introduced by Graftieaux *et*



a) instantaneous vorticity



b) vorticity of the filtered flow



c)  $\Gamma_1$  of the filtered flow, and iso-line  $\Gamma_2 = 2/\pi$  (dashed line)

Figure 2: Instantaneous contours of vorticity and  $\Gamma_1$  on AW1. The three figures are at the same instant.  $y_2$  and  $z_2$  are local coordinates attached to the analysis window.

al.[5]. The first function,  $\Gamma_1$ , is defined at any point  $P$  by:

$$\Gamma_1(P) = \frac{1}{S} \int_{M \in S} \frac{(\mathbf{PM} \times \mathbf{U}_M) \cdot \mathbf{e}_{x_2}}{\|\mathbf{PM}\| \cdot \|\mathbf{U}_M\|} dS \quad (1)$$

where  $S$  is a two-dimensional area around  $P$ ,  $\mathbf{U}_P$  and  $\mathbf{U}_M$  are the velocities at points  $P$  and  $M$ , and  $\mathbf{e}_{x_2}$  is the unit vector normal to the plane (right-handed coordinate system).  $\Gamma_1$  is a non-dimensional scalar, with  $-1 \leq \Gamma_1 \leq 1$ . The constitution of  $\Gamma_1$  is rather intelligible if interpreted as a normalized angular momentum. The extrema of  $\Gamma_1$  allow to detect the vortex centers, and the sign of  $\Gamma_1$  indicates the sense of rotation. In the present study,  $S$  is a box of  $21 \times 21$  points on the regular grid of the analysis window, and extends physically over  $0.07c \times 0.07c$ .  $S$  was chosen to be of the same order of size but smaller than the mean TLV, in coherence with [5], where the influence of this parameter is investigated. For illustration, the  $\Gamma_1$  distribution of the filtered flow at the same instant as before is shown in Figure 2-c). Through the  $\Gamma_1$  distribution, the TLV stands out with respect to the other regions of the flow. The spatial integration over  $S$  provides additional smoothing with respect to the vorticity of the filtered flow. Because  $\Gamma_1$  is normalized, the amplitude of  $\Gamma_1$  is universal ( $\Gamma_1 \in [-1; 1]$ ), and the center of the present TLV is associated with  $\Gamma_1 \approx +1$ . Moreover, the distribution of  $\Gamma_1$  is characterized by a narrow maximum, adapted for a precise detection of the vortex center. Practically, for the treatment of the unsteady snapshots, the TLV center is identified at the  $\Gamma_1$  maximum, with a threshold  $\Gamma_1 \geq 0.85$  imposed for a valid detection.

In their study of TLV unsteadiness from PIV snapshots, Liu *et al.*[8] used the  $\lambda_2$  criterion to locate the instantaneous vortex centers. In the present study, the  $\Gamma_1$  criterion has been chosen instead because it yields two major benefits: the space integration focus on the largest vortices, and the normalization solves the question of the threshold.

A second function was introduced by Graftieaux *et al.* to evaluate the vortex width. The function  $\Gamma_2$  is defined at any point  $P$  by:

$$\Gamma_2(P) = \frac{1}{S} \int_{M \in S} \frac{(\mathbf{PM} \times (\mathbf{U}_M - \mathbf{U}_P)) \cdot \mathbf{e}_{x_2}}{\|\mathbf{PM}\| \cdot \|\mathbf{U}_M - \mathbf{U}_P\|} dS \quad \text{with: } \mathbf{U}_P = \frac{1}{S} \int_{M \in S} \mathbf{U}_M dS \quad (2)$$

Following [5],  $|\Gamma_2| > 2/\pi$  is interpreted as a local predominance of rotation, and the isoline  $|\Gamma_2| = 2/\pi$  is used to define the vortex boundary. In Figure 2-c), the contour  $\Gamma_2 = 2/\pi$  is represented by a dashed line. There are three areas delimited by the dashed line: two large ones, and one small. Nevertheless, the area corresponding to the TLV is clearly identified by the maximum of  $\Gamma_1$  within (cf. color contours).

In fine, the present approach for vortex characterization is much inspired by Graftieaux *et al.*[5], except the scale separation is achieved by filtering instead of Proper Orthogonal Decomposition. This enables to focus the analysis on specific features of the spectrum.

## 4 Analysis of the TLV motion

The vortex center position has been evaluated at each instant with the methodology introduced above ( $\Gamma_1$  maximum of the low-pass filtered flow). The vortex center posi-

tions are indicated with magenta circles in Figure 3, for both analysis windows (AW1 and AW2). At a given grid point, the area of the circle is proportional to the number of matches. For reference, the mean flow is represented by contours of the normal vorticity, the vortex center ( $\times$ ) and the iso-line  $\Gamma_2 = 2/\pi$  (dashed line).

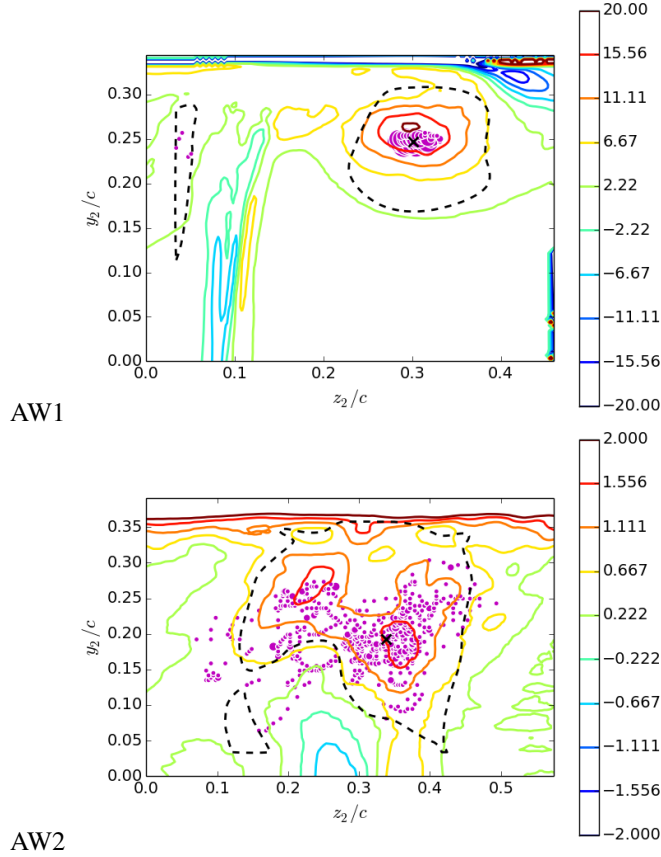


Figure 3: Circles: vortex center positions over time, with area proportional to the number of matches (the same scale is used in AW1 and AW2). Contours: normalized vorticity of the mean flow ( $\Omega_{x2}c/U_{tip}$ ).  $\times$ : mean TLV center. Dashed line: iso-line  $\Gamma_2 = 2/\pi$  of the mean flow.

In AW1, the mean TLV center is located at  $z_2/c = 0.30$  and  $y_2/c = 0.25$ . It is distant from the blade wake, characterized by negative and positive contours of vorticity around  $z_2/c = 0.1$  (in the stationary frame of reference, the rotating blade wake is characterized by higher velocities and the centrifugal force results in positive radial velocities). Over time, the vortex center is shown to move in a well-defined area. The movement amplitude is significant with respect to the vortex radius or the blade chord length:  $\Delta z_2 = 0.05c$  and  $\Delta y_2 = 0.02c$ . This can be clearly interpreted as "vortex wandering", in confirmation of [2].

In AW2, the situation is more complex. First of all, the mean flow is peculiar. In the TLV region, two distinct areas of maximal vorticity are observed: around  $z_2/c = 0.22$  and around  $z_2/c = 0.35$ . These two areas also influence the shape of the  $\Gamma_2 = 2/\pi$  isoline. This two-lobed mean TLV region is probably caused by the interaction of the TLV with the adjacent blade wake. In Figure 1, the streamlines in the TLV of blade (c) are shown to interact with streamlines in the wake of blade (b). The adjacent blade wake is also directly visible in Figure 3-AW2, around  $z_2/c = 0.3$  and  $y_2/c \leq 0.1$ , just below the TLV region, with negative and positive contours of vorticity on each side. The vortex center positions over time are much more scattered in AW2 than in AW1. They cover a region spreading over  $\Delta z_2 \approx 0.2c$  and  $\Delta y_2 \approx 0.15c$ . If one looks at the  $\Gamma_1$  distributions of the different instants separately, the instantaneous topology of the TLV region appears complex, with vortices developing essentially in the two lobes (as shown in Figure 3-AW2) and sometimes coexisting. Moreover, no vortex center is detected for 7.5% of the instants, because the threshold  $\Gamma_1 = 0.85$  is not reached. Overall, the cohesion of TLV appears deteriorated in this region of interaction with the adjacent blade wake. This can be interpreted as "vortex splitting", as observed by Liu *et al.*[8]. In the present case again, it occurs downstream of the vortex wandering region.

At the mean TLV centers of AW1 and AW2 (marked with crosses in Figure 3), the spectra of the  $y_2$  and  $z_2$  components of velocity are calculated, and plotted in Figure 4. In AW1, the spectrum shape is broadband, and a peak stands out at  $f = 1,750\text{Hz}$  on the  $y_2$  component. Since the probe is extracted in the rotating frame of reference, there is no influence of the blade rotation, and this frequency must be related with a natural unsteadiness, as discussed in the previous publication [2]. In terms of Strouhal numbers, this frequency corresponds to  $f \cdot h/U_{tip} = 0.056$  or  $f \cdot c/U_{tip} = 1.02$ . In AW2, the spectrum content is still broadband, with lower levels, and a peak is again visible at  $f = 1,813\text{Hz}$  on the  $z_2$  component, i.e. for Strouhal numbers  $f \cdot h/U_{tip} = 0.058$  or  $f \cdot c/U_{tip} = 1.05$ . The methodology introduced above can be used to investigate this unsteadiness.

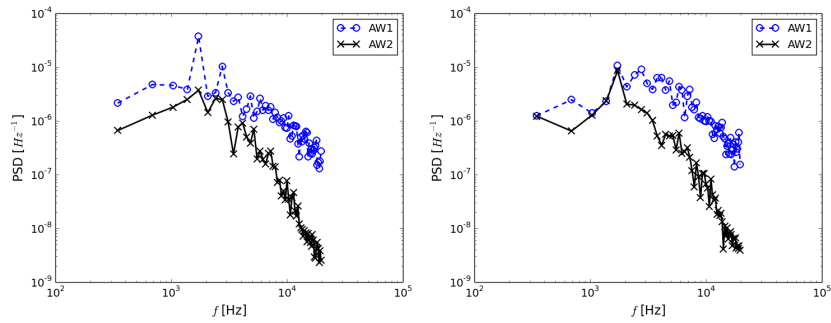


Figure 4: Power spectral densities of the  $y_2$ -component (left) and  $z_2$ -component (right) of velocity, normalized by  $U_{tip}$ , at the mean TLV centers.

A wandering motion has already been identified in AW1 (cf. Figure 3-AW1). In AW2, the movement is disordered and the analysis can be focused on the peak fre-

quency. From the DFT of the unsteady flow in AW2, only the mean flow and the peak frequency are retained, and the reverse Fourier transform is calculated. The  $\Gamma_1$  distributions are then computed for the corresponding periodic unsteady field. In Figure 5, the vortex center positions over time are presented. The peak frequency appears to correspond to a rotating movement of the TLV center. The amplitude is significant:  $\Delta z_2 = 0.06c$  and  $\Delta y_2 = 0.05c$ . This "vortex wandering" emerges from the complex motion observed previously in Figure 3-AW2.

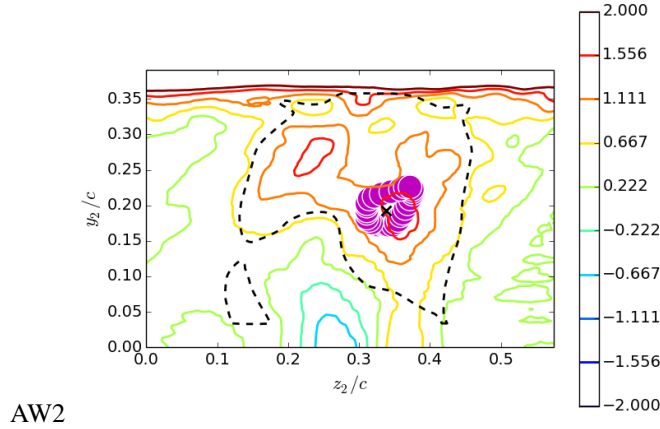


Figure 5: Circles: vortex center positions over time, for the mean flow and the dominant Fourier component, with area proportional to the number of matches (same scale as Figure 3). Contours: normalized vorticity of the mean flow ( $\Omega_{x2}c/U_{tip}$ ).  $\times$ : mean TLV center. Dashed line: iso-line  $\Gamma_2 = 2/\pi$  of the mean flow.

## 5 Conclusion

A methodology has been presented to characterize the motion of a large vortex in a turbulent flow. It combines low-pass filtering with specific vortex identification functions ( $\Gamma_1$  and  $\Gamma_2$ ), for the temporal analysis of the vortex position in selected cross-planes. This approach permits to focus on the largest vortices of the flow at each instant, through normalized criteria. The methodology has been applied to characterize the natural unsteadiness of the TLV in a zonal large-eddy simulation of a fan rotor. Just downstream of the blade trailing edge, the TLV is shown to oscillate pitchwise and the spectrum shows a peak frequency at the Strouhal number  $f \cdot c/U_{tip} = 1.02$ . This phenomenon is interpreted as "vortex wandering". Further downstream, where the TLV interacts with the adjacent blade wake, two lobes of mean vorticity are observed and the movement of the TLV center is much more disordered, over a wider region. This is interpreted as "vortex splitting". However, if only the mean flow and the peak frequency ( $f \cdot c/U_{tip} = 1.05$ ) are retained from the filtering, an oscillation of the TLV is observed again.

## Acknowledgments

The simulation results have been obtained during the project FLOCON, funded by the European Community (7th Framework, No. ACP7-GA-2008-213411). This work was granted access to the HPC resources of CINES under the allocation c2011025039 made by GENCI (Grand Equipement National de Calcul Intensif).

## References

- [1] S. C. C. Bailey and S. Tavoularis. Measurements of the velocity field of a wing-tip vortex, wandering in grid turbulence. *Journal of Fluid Mechanics*, 601:281–315, 2008.
- [2] J. Boudet, A. Cahuzac, P. Kausche, and M. C. Jacob. Zonal large-eddy simulation of a fan tip-clearance flow, with evidence of vortex wandering. *Journal of Turbomachinery*, 137(6), June 2015.
- [3] J. Boudet, J.-F. Monier, and F. Gao. Implementation of a roughness element to trip transition in large-eddy simulation. *Journal of Thermal Science*, 24(1), January 2015.
- [4] F. Gao, W. Ma, G. Zambonini, J. Boudet, X. Ottavy, L. Lu, and L. Shao. Large-eddy simulation of 3-D corner separation in a linear compressor cascade. *Physics of Fluids (1994-present)*, 27(8):085105, August 2015.
- [5] L. Graftieaux, M. Michard, and N. Grosjean. Combining PIV, POD and vortex identification algorithms for the study of unsteady turbulent swirling flows. *Measurement Science and Technology*, 12:1422–1429, 2001.
- [6] B. Lakshminarayana. *Fluid dynamics and heat transfer of Turbomachinery*. John Wiley and Sons, Inc., Hoboken, NJ, 1996.
- [7] E. L ev eque, F. Toschi, L. Shao, and J. P Bertoglio. Shear-improved Smagorinsky model for large-eddy simulation of wall-bounded turbulent flows. *Journal of Fluid Mechanics*, 570:491–502, 2007.
- [8] B. Liu, G. An, X. Yu, and Z. Zhang. Quantitative evaluation of the unsteady behaviors of the tip leakage vortex in a subsonic axial compressor rotor. *Experimental Thermal and Fluid Science*, 79:154–167, December 2016.
- [9] A. Pogorelov, M. Meinke, and W. Schr oder. Cut-cell method based large-eddy simulation of tip-leakage flow. *Physics of Fluids (1994-present)*, 27(7):075106, July 2015.
- [10] D. Tan, Y. Li, I. Wilkes, R. L. Miorini, and J. Katz. Visualization and Time-Resolved Particle Image Velocimetry Measurements of the Flow in the Tip Region of a Subsonic Compressor Rotor. *Journal of Turbomachinery*, 137(4):041007–041007, April 2015.

- [11] H. D. Vo, C. S. Tan, and E. M. Greitzer. Criteria for Spike Initiated Rotating Stall. *Journal of Turbomachinery*, 130, 2008.
- [12] D.C. Wilcox. Reassessment of the scale-determining equation for advanced turbulence models. *AIAA Journal*, 26(11):1299–1310, 1988.
- [13] D. You, M. Wang, P. Moin, and R. Mittal. Vortex Dynamics and Low-Pressure Fluctuations in the Tip-Clearance Flow. *Journal of Fluids Engineering*, 129(8):1002, 2007.